

Bose-Einstein Interference in the Passage of a Jet in a Dense Medium[†]

Cheuk-Yin Wong

Physics Division, Oak Ridge National Laboratory, Oak Ridge, TN 37831

(Dated: May 5, 2019)

When a jet collides coherently with many parton scatterers at very high energies, the Bose-Einstein symmetry with respect to the interchange of the virtual bosons leads to a destructive interference of the Feynman amplitude components in most regions of the momentum transfer phase space but a constructive interference in some other regions of the the momentum transfer phase space. As a consequence, the recoiling scatterers have a tendency to come out collectively along the incident jet direction, each carrying a substantial fraction of the incident jet longitudinal momentum. The manifestation of the Bose-Einstein interference as collective recoils of the scatterers along the jet direction may have been observed in the angular correlations of hadrons associated with a high- p_T trigger in high-energy AuAu collisions at RHIC.

PACS numbers: 25.75.-q 25.75.Dw

I. INTRODUCTION

Recently at RHIC and the LHC, angular correlations of produced hadron pairs in AuAu, PbPb, and pp collisions have been measured to obtain the yield of produced pairs as a function of $\Delta\phi$ and $\Delta\eta$, where $\Delta\phi$ and $\Delta\eta$ are the azimuthal angle and pseudorapidity differences of the produced pair. The correlations appear in the form of a “ridge” that is narrow in $\Delta\phi$ at $\Delta\phi \sim 0$ and $\Delta\phi \sim \pi$, but relatively flat in $\Delta\eta$. They have been observed in high-energy AuAu collisions at RHIC by the STAR Collaboration [1–19], the PHENIX Collaboration [20–24], and the PHOBOS Collaboration [25], with or without a high- p_T trigger [2, 14–18]. They have also been observed in pp and PbPb collisions at the LHC by the CMS Collaboration [26, 27].

Subsequently, among many proposed models [28–70], a momentum kick model was put forth to explain the “ridge” phenomenon [28–35]. The model identifies ridge particles as medium partons, because of the centrality dependence of the ridge particle yield and the similarity of the temperature and baryon/meson ratio of ridge particles with those of the bulk medium particles. The model assumes that these medium partons have an initial rapidity plateau distribution, and they receive a momentum kick predominantly along the jet direction, when they suffer a collision with a jet produced in the collision. The physical contents of the momentum kick model lead to features consistent with experimental observations: (i) the (predominantly) longitudinal momentum kick gives rise to the $\Delta\phi \sim 0$ correlations on the near-side [1, 28, 30], (ii) the medium parton initial rapidity plateau distribution shows up as a ridge along the $\Delta\eta$ direction [1, 3, 28–32, 34, 35], (iii) the displaced parton momentum distribution of the kicked medium partons leads to a peak in

the p_T distribution of the kicked partons [18, 30, 35], and (iv) the kicked medium partons therefore possess a correlation of $|p_{1T}| \sim |p_{2T}| \sim 1$ GeV, without a high- p_T trigger, for both the near side and the away side [18, 35]. The model has been successful in describing extensive sets of triggered associated particle data of the STAR Collaboration, the PHENIX Collaboration, and the PHOBOS Collaboration, over large regions of p_t , $\Delta\phi$, and $\Delta\eta$, in many different phase space cuts and p_T combinations, including dependencies on centralities, dependencies on nucleus sizes, and dependencies on collision energies [28–35].

The phenomenological success of the momentum kick model raises relevant questions about the theoretical foundations for its basic assumptions. While the plateau structure of the medium parton distribution may have its origin in the Wigner function of particles produced in the fragmentation of a string (or flux tube) [33], or in a color-glass condensate [43], the origin of the postulated longitudinal momentum kick in the model poses an interesting puzzle. If each of the jet-(medium parton) collision were a two-body collision, elastic scattering would lead only to a dominantly forward scattering and a small longitudinal momentum transfer. The hard longitudinal momentum kick (of order GeV) in the momentum kick model is unlikely to originate from incoherent two-body collisions.

From an observational viewpoint, the experimental observation that many medium partons come out along the jet direction with $\Delta\phi \sim 0$ implies the presence of collective recoils of the medium partons, each of which must have acquired a substantial longitudinal momentum transfer (momentum kick) along the jet direction from the jet. What is the origin of such collective recoils, in the interaction of the jet with medium partons?

In the multiple collisions of a fast particle p of momentum $p = (p_0, \mathbf{p})$ with many medium particles, it is instructive to find out the criteria to determine whether the series of multiple collisions are coherent or incoherent. For such a purpose, we consider first the collision of the fast particle p with one of medium particles a in

[†]Based in part on a talk presented at the Fourteenth Meeting of the Chinese Nuclear Physical Society in Intermediate and High Energy Nuclear Physics, Qufu, Shandong, China, October 20–24, 2011.

the reaction $p + a \rightarrow p' + a'$, with the emission and absorption of a virtual boson of momentum q between p and a . For definiteness, we can study this collision in the medium center-of-mass frame. The six degrees of freedom of the final state in $d\mathbf{p}'d\mathbf{a}'$ are constrained by the four-dimensional conservation of energy and momentum, leaving only two independent degrees of freedom. We can choose the two independent degrees of freedom to be the magnitude of the transverse momentum transfer q_T and the azimuthal angle ϕ . The longitudinal momentum transfer q_z is then a dependent variable. If we consider the two-body scattering as obtained from a virtual boson exchange potential with a transverse momentum transfer q_T , then q_z is given by $q_z \sim q_T^2/2p_0$. We can therefore define a longitudinal coherence length Δz_{coh} that gives the uncertainty in the longitudinal vertex location at which the virtual boson is emitted. By the uncertainty principle, the longitudinal coherence length Δz_{coh} is $\hbar/q_z \sim 2\hbar p_0/q_T^2$. The time it takes for the fast particle to travel the distance of the longitudinal coherence length, $2p_0\hbar/q_T^2c$, can also be called the virtual boson formation time.

The comparison of the longitudinal coherence length Δz_{coh} with the mean free path λ of the jet in the scatterer medium provides the criteria to determine the nature of the multiple scattering process. If $\Delta z_{\text{coh}} \ll \lambda$, then a single two-body collision is completed before another two-body collision begins, and the multiple collisions of the jet with many medium particles is a series of incoherent collisions. If $\Delta z_{\text{coh}} \gg \lambda$, then a single two-body collision is not completed before another one begins, and the set of multiple collisions of the jet with the medium partons is a set of coherent collisions.

For a typical transverse momentum transfer of $q_T \sim 0.4$ GeV/c and an incident jet momentum of $p_0 \sim 10$ GeV/c at RHIC [20], the longitudinal coherent length Δz_{coh} is of order 25 fm. On the other hand, medium partons at the early stage of the collision when the jets are present are within a radius of the order of the nuclear radius R (of many fermi), which in turn is much greater than the mean free path λ between jet-scatterer collisions. In high-energy nuclear collisions, $\Delta z_{\text{coh}} \gg R \gg \lambda$.

As $\Delta z_{\text{coh}} \gg \lambda$, the multiple collisions of a jet with medium partons along its path constitute a set of coherent collisions. For the same final state, there are uncertainties in the locations of the vertices along Δz_{coh} at which various virtual bosons are emitted. By Bose-Einstein symmetry, the scattering amplitude is then the sum of all amplitudes with all interchanges of the virtual boson vertices. The summation of these amplitudes and its accompanying interference constitute the Bose-Einstein interference in the passage of the jet in the dense medium.

In this connection of Bose-Einstein interference, we note the many-body Bose-Einstein interference effects in high-energy QED and QCD collisions observed previously by many workers [71–78]. In the emission or absorption of n identical bosons from an energetic fermion

in Abelian and non-Abelian gauge theories leading to an on-mass-shell final fermion, the Bose-Einstein symmetry with respect to the interchange of virtual bosons leads to a sum of a large set of Feynman amplitudes that turns out very simply to be a product of delta functions. These distributions may be thought of as peaked interference patterns produced by the coherent addition of various symmetrized broad Feynman amplitude components [78]. In the collision of two fermions, the sum of the ladder and cross-ladder diagrams also exhibits remarkable Bose-Einstein interference leading to similar products of delta functions and the eikonal approximation [71–78].

We would like to study similar interference effects for the case of the multiple collisions of a jet parton with many parton scatterers. We wish to explore whether such a Bose-Einstein symmetrization interference may be the origin of the longitudinal momentum kick. As the interference arises from the coherent collision of more than one particle, it is clearly a many-body effect that is beyond the treatment of a series of incoherent two-body collisions.

The interference of Feynman amplitudes is only one of the effects of coherent collisions. There is another important effect of coherent collisions which shows up as an increase in the number of degrees of freedom. In a sequence of n incoherent two-body collisions, there are two degrees of freedom in each two-body collision, which can be chosen to be $\mathbf{q}_{iT} = (q_{iT}, \phi_i)$. The sequence of n incoherent two-body collisions contains only $2n$ transverse momentum transfer degrees of freedom, $\{\mathbf{q}_{1T}, \mathbf{q}_{2T}, \mathbf{q}_{3T}, \dots, \mathbf{q}_{nT}\}$. The longitudinal momentum transfer in each individual jet-parton collision is a dependent variable, depending on the corresponding transverse momentum transfer as $q_{iz} = |\mathbf{q}_{iT}|^2/2p_0$. In contrast, in the case of coherent collisions of the jet with n particles, there are $3n - 1$ degrees of freedom, after the $3(n + 1)$ degrees of freedom are reduced by the constraints of the conservation of energy and momentum. The degrees of freedom increases from $2n$ for incoherent collision to $3n - 1$ for coherent collisions. We can choose the $3n - 1$ independent variables to be $\{\mathbf{q}_{1T}q_{1z}, \mathbf{q}_{2T}q_{2z}, \mathbf{q}_{3T}q_{3z}, \dots, \mathbf{q}_{nT}q_{nz}\}$ for coherent collisions, subject to a single condition of an overall energy conservation. Thus in the case of coherent collisions, the set of longitudinal momentum transfers, $\{q_{iz}, i = 1, 2, \dots, n\}$, can also be independent variables with their own distribution functions, sharing the longitudinal momentum of the incident jet. These q_{iz} degrees of freedom allow the medium partons to acquire substantial fractions of the longitudinal momentum of the incident jet, as we shall demonstrate in Section III of this paper.

In the remaining parts of the manuscript, we shall consider implicitly only coherent multiple collisions of the jet with medium partons. In Section II, we examine (coherent) multiple collisions of an energetic fermion with two fermion scatterers in the Abelian gauge theory to discuss how the Bose-Einstein symmetry in the Feynman amplitude can lead to a destructive interference over most

regions of phase space but a constructive interference in some other regions of phase space. In Section III, we study the cross section for such a multiple collision process. We examine the consequences of the constraints on the recoils of the scatterers and find that the scatterers tend to come out collectively along the incident jet direction, each scatterer acquiring a significant fraction of the longitudinal momentum of the incident jet. In Section IV, we examine the case for the multiple collisions of an energetic fermion with fermion scatterers in the non-Abelian gauge theory. In Section V, we generalize our considerations to the collision of a gluon jet on quark scatterers. In Section VI, we examine the collision of a gluon or a fermion jet on gluon scatterers. In Section VII, we study the longitudinal momentum distribution for gluon scatterers and distinguish it from the longitudinal momentum distribution for quark scatterers. In Section VIII, we examine the signatures of the Bose-Einstein interference in the passage of a jet in a medium and compare these signatures with experimental data. In Section IX, we present our conclusions and discussions.

II. BOSE-EINSTEIN INTERFERENCE OF THE FEYNMAN AMPLITUDES

We consider a jet p passing through a dense medium and making (coherent) multiple collisions with medium partons. The assembly of medium partons has an initial momentum distribution. We choose to work in the center-of-momentum frame of the assembly of parton scatterers $\{a_1, a_2, \dots, a_n\}$. We select the z -axis to be along the momentum of the incident jet.

As an illustration of the salient features of the interference of the Feynman amplitude components, we consider first multiple collisions of a fermion p with two fermion scatterers a_1 and a_2 in $p + a_1 + a_2 \rightarrow p' + a'_1 + a'_2$. For simplicity, we assume the rest masses of the fermions to be the same. We study this problem in the Abelian gauge theory in this section and in the non-Abelian gauge theory in Section IV. We shall consider the collision of gluons in Section V.

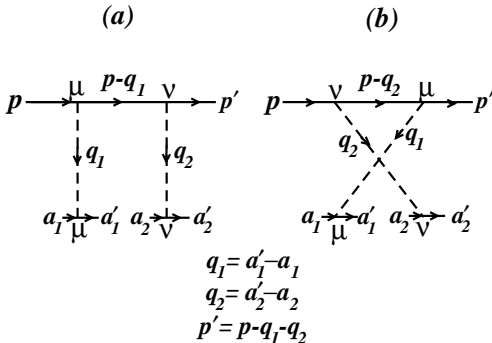


FIG. 1: Feynman diagrams for the collision of a fast fermion p with medium fermions a_1, a_2 , with the emission and absorption of virtual bosons of momenta q_1 and q_2 .

The reaction process is described by the two Feynman diagrams in Fig. (1). Using the Feynman rules and overall factors as given in Ref. [72], the amplitude M_1 for Feynman diagram 1(a) is given by

$$M_1 = -g^4 \bar{u}(p') \gamma_\nu \frac{1}{\not{p} - \not{q}_1 - m + i\epsilon'} \gamma_\mu u(p) \times \frac{1}{q_2^2} \bar{u}(a'_2) \gamma_\nu u(a_2) \frac{1}{q_1^2} \bar{u}(a'_1) \gamma_\mu u(a_1). \quad (1)$$

There is an additional amplitude M_2 in Feynman diagram 1(b), obtained by making a symmetrized permutation of the bosons in diagram 1(a),

$$M_2 = -g^4 \bar{u}(p') \gamma_\mu \frac{1}{\not{p} - \not{q}_2 - m + i\epsilon'} \gamma_\nu u(p) \times \frac{1}{q_2^2} \bar{u}(a'_2) \gamma_\nu u(a_2) \frac{1}{q_1^2} \bar{u}(a'_1) \gamma_\mu u(a_1). \quad (2)$$

We consider the high-energy limit

$$\{p_0, |\mathbf{p}|, p'_0, |\mathbf{p}'|\} \gg \{|\mathbf{a}_i|, q_0, |\mathbf{q}_i|\} \gg m, \text{ for } i = 1, 2. \quad (3)$$

We assume conservation of helicity in high-energy collisions. In this limit, we have approximately [72]

$$\bar{u}(a') \gamma_\mu u(a) \sim \sqrt{\frac{a_0 + m}{a'_0 + m}} \frac{a'_\mu}{2m} + \sqrt{\frac{a'_0 + m}{a_0 + m}} \frac{a_\mu}{2m} \equiv \frac{\tilde{a}_\mu}{m} \quad (4)$$

$$\frac{1}{\not{p} - \not{q}_1 - m + i\epsilon'} \gamma_\nu u(p) \sim -\frac{\not{p} - \not{q}_1 + m}{2p \cdot q_1 - i\epsilon} \gamma_\nu u(p), \quad (5)$$

$$\gamma_\nu (\not{p} - \not{q}_1 + m) \gamma_\mu \sim \gamma_\nu \not{p} \gamma_\mu \sim 2p_\mu \gamma_\nu \sim \frac{2p_\nu p_\mu}{m}, \quad (6)$$

where ϵ is a small positive quantity.

We shall be interested in the case in which the fermion p' remains on the mass shell after the collision. In the high-energy limit, the mass-shell condition for the fermion p' after the collision can be written as

$$(p - q_1 - q_2)^2 - m^2 \sim -2p \cdot q_1 - 2p \cdot q_2 \sim 0, \quad (7)$$

which has important consequences in the cancellation of the real parts of the Feynman amplitude components in diagrams 1(a) and 1(b).

The amplitude M_1 from diagram 1(a) is

$$M_1 \sim g^4 \frac{2p \cdot \tilde{a}_1 2p \cdot \tilde{a}_2}{2m^3} \frac{1}{2p \cdot q_1 - i\epsilon} \frac{1}{q_2^2} \frac{1}{q_1^2}, \quad (8)$$

which is non-zero for a large region of $p \cdot q_1$. The fermion propagator factor in Eq. (8) can be written as

$$\mathcal{M}_1 \equiv \frac{1}{2p \cdot q_1 - i\epsilon} = \frac{2p \cdot q_1}{(2p \cdot q_1)^2 + \epsilon^2} + i\Delta(2p \cdot q_1), \quad (9)$$

where

$$\Delta(2p \cdot q_1) = \frac{\epsilon}{(2p \cdot q_1)^2 + \epsilon^2}. \quad (10)$$

The function $\Delta(2p \cdot q_1)$ approaches the Dirac delta function $\delta(2p \cdot q_1)$ in the limit $\epsilon \rightarrow 0$. Similarly, the amplitude M_2 from diagram 1(b) is

$$M_2 \sim g^4 \frac{2p \cdot \tilde{a}_1 2p \cdot \tilde{a}_2}{2m^3} \frac{1}{2p \cdot q_2 - i\epsilon} \frac{1}{q_2^2} \frac{1}{q_1^2}, \quad (11)$$

which is proportional to

$$\mathcal{M}_2 \equiv \frac{1}{2p \cdot q_2 - i\epsilon} = \frac{2p \cdot q_2}{(2p \cdot q_2)^2 + \epsilon^2} + i\Delta(2p \cdot q_2). \quad (12)$$

The total amplitude M is the symmetrized sum of the two amplitude components, $M = M_1 + M_2$. In the high-energy limit, the sum of the two Feynman amplitude components is

$$M \sim g^4 \frac{2p \cdot \tilde{a}_1 2p \cdot \tilde{a}_2}{2m^3} \left(\frac{1}{2p \cdot q_1 - i\epsilon} + \frac{1}{2p \cdot q_2 - i\epsilon} \right) \frac{1}{q_2^2} \frac{1}{q_1^2}. \quad (13)$$

Because of the mass-shell condition (7), the amplitudes M_1 and M_2 are correlated with each other and they destructively cancel each other in most of the region of $p \cdot q_1$ and $p \cdot q_2$. However they interfere constructively at $p \cdot q_1 \sim 0$ and $p \cdot q_2 \sim 0$, to result in sharp distributions at these two locations,

$$\frac{1}{2p \cdot q_1 - i\epsilon} + \frac{1}{2p \cdot q_2 - i\epsilon} = i\Delta(2p \cdot q_1) + i\Delta(2p \cdot q_2). \quad (14)$$

Upon multiplying the mass-shell condition (7) that can be explicitly written in terms of a Δ -function, the sum amplitude M becomes

$$\begin{aligned} & M \Delta(2p \cdot q_1 + 2p \cdot q_2) \\ & \sim g^4 \frac{2p \cdot \tilde{a}_1 2p \cdot \tilde{a}_2}{2m^3} 2i\Delta(2p \cdot q_1)\Delta(2p \cdot q_2) \frac{1}{q_2^2} \frac{1}{q_1^2}. \end{aligned} \quad (15)$$

Thus, the Bose-Einstein symmetrization of the bosons in the Feynman amplitude components leads to interesting interferences in the collision of an energetic fermion with two fermion scatterers.

We consider next the case of the (coherent) multiple collisions of a fast fermion with three fermion scatterers in the reaction $p + a_a + a_2 + a_3 \rightarrow p' + a'_1 + a'_2 + a'_3$. The Feynman diagrams for the multiple collisions process are shown in Fig. 2.

In the high-energy limit, the Feynman amplitude for the collision is

$$\begin{aligned} M &= g^6 \frac{2p \cdot \tilde{a}_1 2p \cdot \tilde{a}_2 2p \cdot \tilde{a}_3}{2m^5 q_1^2 q_2^2 q_3^2} \\ &\times \left\{ \left[\frac{1}{(2p \cdot q_1 - i\epsilon)(2p \cdot q_1 + 2p \cdot q_2 - i\epsilon)} \right. \right. \\ &\quad \left. \left. + \frac{1}{(2p \cdot q_2 - i\epsilon)(2p \cdot q_1 + 2p \cdot q_2 - i\epsilon)} \right] \right. \\ &\quad \left. + \left[\frac{1}{(2p \cdot q_2 - i\epsilon)(2p \cdot q_2 + 2p \cdot q_3 - i\epsilon)} \right] \right\} \end{aligned}$$

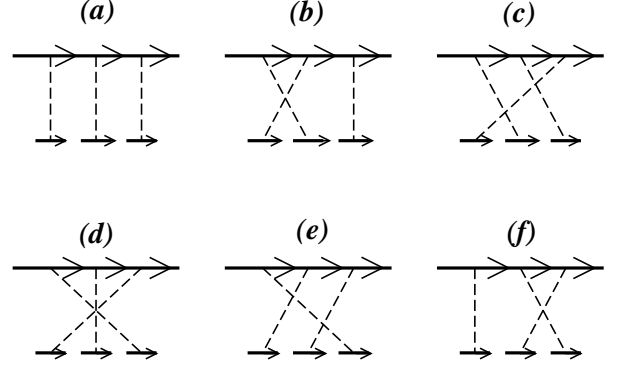


FIG. 2: Feynman diagrams for the multiple collisions of a fast fermion with three medium fermions in different permutations of the exchanged bosons.

$$\begin{aligned} & + \frac{1}{(2p \cdot q_3 - i\epsilon)(2p \cdot q_2 + 2p \cdot q_3 - i\epsilon)} \Big] \\ & + \left[\frac{1}{(2p \cdot q_3 - i\epsilon)(2p \cdot q_3 + 2p \cdot q_1 - i\epsilon)} \right. \\ & \quad \left. + \frac{1}{(2p \cdot q_1 - i\epsilon)(2p \cdot q_3 + 2p \cdot q_1 - i\epsilon)} \right] \Big\}. \end{aligned} \quad (16)$$

Each amplitude term in the curly bracket contains a distribution that is non-zero in various regions of $p \cdot q_i$. These Feynman amplitude components interfere destructively among themselves leading to a vanishing amplitude at most regions but constructively at $p \cdot q_i \sim 0$. To see how the interference and cancellation works, one can expand terms in the curly bracket in Eq. (16) in powers of ϵ , multiplying M by the a Δ -function representing the mass-shell condition for the final particle p' , and collect terms of the same order. One finds that terms of power ϵ and ϵ^2 cancel, and the leading term is ϵ^3 yielding the result

$$\begin{aligned} & M \Delta(2p \cdot q_1 + 2p \cdot q_2 + 2p \cdot q_3) \\ &= g^6 \frac{2p \cdot \tilde{a}_1 2p \cdot \tilde{a}_2 2p \cdot \tilde{a}_3}{2m^5 q_1^2 q_2^2 q_3^2} \\ &\quad \times 3i^2 \Delta(2p \cdot q_1) \Delta(2p \cdot q_2) \Delta(2p \cdot q_3). \end{aligned} \quad (17)$$

Generalizing to the case of the coherent collision with n fermions [72], the sum amplitude including all the symmetric permutations of the exchanged bosons is

$$\begin{aligned} & M \Delta \left(\sum_{i=1}^n 2p \cdot q_i \right) \\ &= g^{2n} \frac{\prod_{i=1}^n 2p \cdot \tilde{a}_i}{2m^{2n-1} q_1^2 q_2^2 q_3^2 \dots q_n^2} n i^{n-1} \prod_{i=1}^n \Delta(2p \cdot q_i). \end{aligned} \quad (18)$$

We can express the amplitude in Eq. (18) alternatively as

$$M = \frac{i^{n-1} g^{2n} \prod_{i=1}^n 2p \cdot \tilde{a}_i}{2m^{2n-1}} \frac{D(q_1, q_2, \dots, q_n)}{\prod_{i=1}^n q_i^2}, \quad (19)$$

where D is a sum of products of Δ functions

$$D(q_1, q_2, \dots, q_n) = \sum_{j=1} \left\{ \prod_{i=1, i \neq j} \Delta(2p \cdot q_i) \right\}, \quad (20)$$

and the momentum transfers q_i implicitly obey the on-mass-shell condition of the fermion p' ,

$$\sum_{i=1}^n p \cdot q_i = 0. \quad (21)$$

Equation (18) for the Feynman amplitude as a product of delta functions of $2p \cdot q_i$, is similar to previous results obtained for the emission of many real photons or gluons in bremsstrahlung and for the sum of ladder and cross-ladder amplitudes in the collision of two fermions [71–78].

III. CONSEQUENCES OF THE BE INTERFERENCE ON THE RECOIL OF FERMION SCATTERERS

We study the reaction $p + a_1 + a_2 + \dots + a_n \rightarrow p' + a'_1 + a'_2 + \dots + a'_n$, in the center-of-momentum frame of the assembly of scatterers $\{a_1, a_2, \dots, a_n\}$. The differential cross section for the reaction is

$$d\sigma = \frac{1}{v_p - \langle v \rangle} \frac{|M|^2}{4p_0 \langle a_0 \rangle} (2\pi)^4 \delta^4(p' + \sum_{i=1}^n q_i - p) \times \frac{d^3 p'}{(2\pi)^3 2p'_0} \prod_{i=1}^n \frac{d^3 a'_i}{(2\pi)^3 2a'_{i0}}, \quad (22)$$

where v_p is the velocity of p , $\langle v \rangle$ and $\langle a_0 \rangle$ are the average velocity and energy of the target scatterers, respectively. We change variables from \mathbf{a}'_i to \mathbf{q}_i ,

$$d\mathbf{a}'_i = d(\mathbf{a}_i + \mathbf{q}_i) = d\mathbf{q}_i = dq_{iz} d\mathbf{q}_{iT}, \quad (23)$$

and we can integrate over \mathbf{p}' to obtain

$$d\sigma = \frac{2\pi}{2(2\pi)^{3n}} \frac{1}{v_p - \langle v \rangle} \frac{|M|^2}{4p_0 \langle a_0 \rangle} \delta(p'_0 + \sum_{i=1}^n q_{i0} - p_0) \times \frac{1}{p'_0} \prod_{i=1}^n \frac{dq_{iz} d\mathbf{q}_{iT}}{2a'_{i0}}. \quad (24)$$

The cross section is then given by

$$d\sigma = C |D(q_1, q_2, \dots, q_n)|^2 \frac{1}{p'_0} \prod_{i=1}^n \frac{(2p \cdot \tilde{a}_i)^2 dq_{iz} d\mathbf{q}_{iT}}{2a'_{i0} q_i^4} \times \delta(p'_0 + \sum_{i=1}^n q_{i0} - p_0), \quad (25)$$

where C is a constant given by

$$C = \frac{2\pi}{2(2\pi)^{3n}} \frac{1}{v_p - \langle v \rangle} \frac{1}{4p_0 \langle a_0 \rangle} \left| \frac{g^{2n}}{2m^{2n-1}} \right|^2. \quad (26)$$

We can study the probability distribution for the momentum transfers \mathbf{q}_i by examining Eq. (25). The distribution $D(q_1, q_2, \dots, q_n)$ contains a product of $\Delta(p \cdot q_i)$ functions that are sharply peaked at $p \cdot q_i = 0$ for $i = 1, 2, \dots, n$. Each of the $\Delta(2p \cdot q_i)$ distribution corresponds to a constraint

$$2p \cdot q_i = p_+ q_{i-} + p_- q_{i+} - 2\mathbf{p}_T \cdot \mathbf{q}_{iT} = 0, \quad (27)$$

which is satisfied by

$$q_{i-} = \frac{1}{p_+} (2\mathbf{p}_T \cdot \mathbf{q}_{iT} - p_- q_{i+}). \quad (28)$$

In the high energy limit, $p_0 \sim p_z$, $p_+ \equiv p_0 + p_z \sim 2p_z$, and $p_- \equiv p_0 - p_z \sim 0$. We have therefore $p_+ \gg |\mathbf{p}_T|, |\mathbf{q}_i|, p_-$ and the quantity q_{i-} is close to zero,

$$q_{i-} \equiv q_0 - q_z \sim 0. \quad (29)$$

As a consequence, the denominators of the boson propagator in Eq. (25) becomes

$$q_i^2 = q_{i+} q_{i-} - |\mathbf{q}_{iT}|^2 \approx -|\mathbf{q}_{iT}|^2, \quad (30)$$

which is predominantly transverse in nature. The reaction has a high probability for the occurrence of small values of $|\mathbf{q}_{iT}|$.

To find the probability distribution for the longitudinal momentum transfer q_{iz} , we introduce the fractional longitudinal momentum kick

$$x_i = \frac{q_{iz}}{p_z}, \quad (31)$$

then

$$dq_{iz} = p_z dx_i. \quad (32)$$

For $p_z \gg \{|\mathbf{q}_i|, |\mathbf{a}_i|, m\}$ in the high-energy limit, we have approximately

$$p'_0 \sim p_z (1 - \sum_{i=1}^n x_i). \quad (33)$$

To investigate the x_i dependence of the factor $(2p \cdot \tilde{a}_i)^2 / 2a'_{i0}$ in Eq. (25), we note from Eq. (4) that \tilde{a}_i can be written as a function of q_i and a_i ,

$$\tilde{a}_i \sim \sqrt{\frac{a_{i0} + m}{a'_{i0} + m}} \frac{q_i}{2} + \frac{a'_{i0} + m + a_{i0} + m}{\sqrt{(a'_{i0} + m)(a_{i0} + m)}} \frac{a_i}{2}. \quad (34)$$

Because of the $\Delta(2p \cdot q_i)$ constraint, the factor $(2p \cdot \tilde{a}_i)^2 / 2a'_{i0}$ in Eq. (25) becomes

$$\frac{(2p \cdot \tilde{a}_i)^2}{2a'_{i0}} \sim \frac{(a'_{i0} + a_{i0})^2 (p \cdot a_i)^2}{2(a'_{i0})^2 a_{i0}} \equiv \kappa_i \frac{(p \cdot a_i)^2}{a_{i0}}. \quad (35)$$

The fermion scatterers can possess different initial energies a_{i0} at the moment of their collisions with the energetic jet. In the case when $a_{i0} \ll q_{i0}$, the factor κ_i

approaches $1/2 + O(a_{i0}/q_{iz})$ with $(a_{i0}/q_{iz}) \ll 1$. In the other extreme when $a_{i0} \gg q_{i0}$, the factor κ approaches $2 + O(q_{iz}/a_{i0})$ with $(q_{iz}/a_{i0}) \ll 1$. Therefore we can neglect the dependence of the κ_i factor on q_{iz} (or x_i) in our first approximate estimate. We obtain from Eq. (25)

$$d\sigma = Cp_z^{n-1} \left(\prod_{i=1}^n \frac{\kappa_i(p \cdot a_i)^2}{a_{i0}} \right) |D(q_1, q_2, q_3, \dots, q_n)|^2 \times \frac{dx_1 dx_2 \dots dx_n}{(1 - \sum_{i=1}^n x_i)} \delta(p^0 - p'^0 - \sum_{i=1}^n q_i^0) \prod_{i=1}^n \frac{dq_{iT}}{q_{iT}^4}. \quad (36)$$

In the above expression, the function $D(q_1, q_2, \dots, q_n)$ serves to provide the constraint on $q_{i0} \sim q_{iz}$, but otherwise places no constraint on the magnitude of q_{iz} (or x_i).

The probability for the x_i variables is given by the unnormalized distribution

$$\frac{dP}{dx_1 dx_2 \dots dx_n} = \frac{1}{(1 - x_1 - x_2 - \dots - x_n)}. \quad (37)$$

The singularities at $|\mathbf{q}_{iT}| \sim 0$ and $(1 - x_1 - \dots - x_n) \sim 0$ in Eq. (36) correspond to the case of infrared instabilities that may be renormalized, and a momentum cut-off Λ_{cut} may be introduced.

There is a significant probability for the occurrence of x_i substantially greater than zero. On average, the fraction of momentum transfers x_i for different scatterers are approximately the same. Then as far as x_i is concerned, the unnormalized distribution on the average is

$$\left. \frac{dP}{dx_i} \right|_{x_j=x_i, j=1, \dots, n} \sim \frac{1}{(1 - nx_i)^{1/n}}. \quad (38)$$

In Fig. 3, we plot this “average” dP/dx_i as a function of x_i for the case of $n = 4$ and 6 . The probability distribution is approximately confined to the region $0 < x_i < 1/n$ and has a peak at $1/n$.

We can estimate the average longitudinal momentum fraction for the distribution of Eq. (38) in Fig. 3 for n scatterers. We have $x_{\text{imin}} = \frac{\Lambda_{\text{cut}}}{p_z}$,

$$x_{\text{imax}} = \frac{1}{n} \left(1 - \frac{\Lambda_{\text{cut}}}{p_z} \right), \quad (39)$$

and we obtain

$$\langle x_i \rangle = \frac{1}{n} + \frac{n-1}{n^2(2-1/n)} \left\{ \left(\frac{\Lambda_{\text{cut}}}{p_z} \right)^{2-\frac{1}{n}} - \left(1 - \frac{\Lambda_{\text{cut}}}{p_z} \right)^{2-\frac{1}{n}} \right\} \quad (40)$$

For $\Lambda_{\text{cut}}/p_z \ll 1$, we get

$$\langle x_i \rangle = \frac{1}{2n-1}. \quad (41)$$

The above estimate is based on the assumption that in the high-energy limit, p' is not significantly different from p . It may not be applicable in the regions of x_i close to

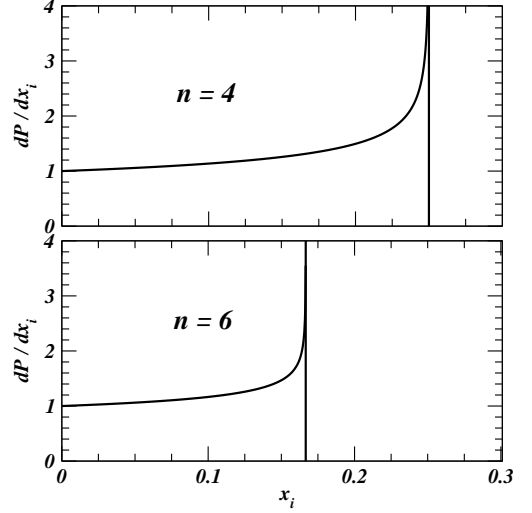


FIG. 3: The average dP/dx_i for the longitudinal momentum transfer in units of the incident longitudinal momentum, $x_i = q_{iz}/p_z$, in the collision of a fast fermion with $n=4$ and 6 fermions.

$1/n$ for which p' is substantially reduced from p . Therefore, the estimate of $\langle x_i \rangle$ given above can only be considered as an upper limit. On the other hand, the probability distribution is relatively flat for small values of x_i and it increases monotonically as x_i increases. If the probability distribution dP/dx_i were flat as a function of x_i , the average $\langle x_i \rangle$ would be $1/2n$. The lower limit of $\langle x_i \rangle$ should be $1/2n$, which leads the range of expected average $\langle x_i \rangle$ given by

$$\frac{1}{2n} \lesssim \langle x_i \rangle \lesssim \frac{1}{2n-1}. \quad (42)$$

The above estimate indicates that in the passage of an energetic fermion making coherent collisions with medium partons, there is a collective quantum many-body effect arising from Bose-Einstein interference such that the fermion scatterers emerge in the forward direction, each receiving a substantial fraction of the forward longitudinal momentum of the incident particle inversely proportional to the number of scatterers.

IV. BOSE-EINSTEIN INTERFERENCE FOR COLLISIONS IN NON-ABELIAN THEORY

We consider first a quark jet making coherent collisions with quarks a_1 and a_2 in the reaction $p + a_1 + a_2 \rightarrow p' + a'_1 + a'_2$, in the non-Abelian theory. We shall neglect four-particle vertices and loops, which are of higher-orders. The Feynman diagrams are then the same as those in Fig. 1. One associates each quark vertex with a color matrix $T_{a,b}^{(p,1,2)}$ where the superscript $p, 1$, or 2 identifies the quark p, a_1 , or a_2 , and the subscript a or b gives the $SU(3)$ color matrix index.

The amplitude M_1 for Feynman diagram 1(a) is

$$M_1 = -g^4 \bar{u}(\mathbf{p}') T_b^{(p)} \gamma_\nu \frac{1}{\not{p} - \not{q}_1 - m + i\epsilon'} T_a^{(p)} \gamma_\mu u(\mathbf{p}) \\ \times \frac{1}{q_2^2} \bar{u}(\mathbf{a}_2') T_b^{(2)} \gamma_\nu u(\mathbf{a}_2) \frac{1}{q_1^2} \bar{u}(\mathbf{a}_1') T_a^{(1)} \gamma_\mu u(\mathbf{a}_1). \quad (43)$$

The amplitude M_2 in diagram 1(b) is

$$M_2 = -g^4 \bar{u}(\mathbf{p}') T_a^{(p)} \gamma_\mu \frac{1}{\not{p} - \not{q}_2 - m + i\epsilon'} T_b^{(p)} \gamma_\nu u(\mathbf{p}) \\ \times \frac{1}{q_2^2} \bar{u}(\mathbf{a}_2') T_b^{(2)} \gamma_\nu u(\mathbf{a}_2) \frac{1}{q_1^2} \bar{u}(\mathbf{a}_1') T_a^{(1)} \gamma_\mu u(\mathbf{a}_1). \quad (44)$$

In the high-energy limit, the sum of the Feynman amplitude is

$$M \sim -g^4 \frac{2p \cdot \tilde{a}_1 2p \cdot \tilde{a}_2}{2m^3 q_1^2 q_2^2} \\ \times \left(\frac{T_b^{(p)} T_a^{(p)} T_b^{(2)} T_a^{(1)}}{2p \cdot q_1 - i\epsilon} + \frac{T_a^{(p)} T_b^{(p)} T_b^{(2)} T_a^{(1)}}{2p \cdot q_2 - i\epsilon} \right). \quad (45)$$

We recognize the propagators in Eq. (45) as \mathcal{M}_1 and \mathcal{M}_2 ,

$$\mathcal{M}_1 = \frac{1}{2p \cdot q_1 - i\epsilon}, \quad (46)$$

$$\mathcal{M}_2 = \frac{1}{2p \cdot q_2 - i\epsilon}, \quad (47)$$

as given by Eqs. (9) and (12). We can rewrite the product of the color matrices as

$$T_b^{(p)} T_a^{(p)} = \frac{1}{2} \left([T_b^{(p)}, T_a^{(p)}]_+ + [T_b^{(p)}, T_a^{(p)}]_- \right), \quad (48)$$

$$T_a^{(p)} T_b^{(p)} = \frac{1}{2} \left([T_b^{(p)}, T_a^{(p)}]_+ - [T_b^{(p)}, T_a^{(p)}]_- \right). \quad (49)$$

The Feynman amplitude is then

$$M \sim -g^4 \frac{2p \cdot \tilde{a}_1 2p \cdot \tilde{a}_2}{2m^3 q_1^2 q_2^2} \left\{ (\mathcal{M}_1 + \mathcal{M}_2) \frac{[T_b^{(p)}, T_a^{(p)}]_+ + T_b^{(2)} T_a^{(1)}}{2} \right. \\ \left. + (\mathcal{M}_1 - \mathcal{M}_2) \frac{[T_b^{(p)}, T_a^{(p)}]_- - T_b^{(2)} T_a^{(1)}}{2} \right\}. \quad (50)$$

The first term inside the curly bracket has the same space-time structure as what one obtains in the Abelian theory. It is given by the Abelian Feynman amplitude in Section II, multiplied by the color factor $[T_b^{(p)}, T_a^{(p)}]_+ + T_b^{(2)} T_a^{(1)}/2$. The sum of \mathcal{M}_1 and \mathcal{M}_2 leads to sharp distributions at $p \cdot q_1 \sim 0$ and $p \cdot q_2 \sim 0$,

$$\mathcal{M}_1 + \mathcal{M}_2 = i\Delta(2p \cdot q_1) + i\Delta(2p \cdot q_2). \quad (51)$$

The second term is new and occurs only in the non-Abelian theory, as it involves the commutator of $T_b^{(p)}$ and $T_a^{(p)}$. It also involves the difference of \mathcal{M}_1 and \mathcal{M}_2 in which the sharp distributions cancel each other, leaving a broad distribution,

$$\mathcal{M}_1 - \mathcal{M}_2 = \frac{4p \cdot q_1}{(2p \cdot q_1)^2 + \epsilon^2}. \quad (52)$$

From the above analysis, we find that the color degrees of freedom in QCD brings in additional properties to the Feynman amplitude. Bose-Einstein symmetry with respect to the interchange of gluons in QCD involves not only the space-time exchange symmetry but also color index exchange symmetry. The total exchange symmetry can be attained with symmetric space-time amplitudes and symmetric color index factors as in the first $\mathcal{M}_1 + \mathcal{M}_2$ term in Eq. (50). The total symmetry can also be attained with space-time antisymmetry and color index antisymmetry, as in the second $\mathcal{M}_1 - \mathcal{M}_2$ term in Eq. (50).

We consider next the case for the collision of a quark jet with three quark scatterers in the reaction $p + a_a + a_2 + a_3 \rightarrow p' + a_1' + a_2' + a_3'$ in the non-Abelian theory. The Feynman diagrams for the collision process are the same as those in Fig. 2 where we associate the color matrices $T_a^{(1)}, T_b^{(2)}, T_c^{(3)}$ of color indices a, b, c with fermion scatterers a_1, a_2 and a_3 respectively. In the high-energy limit, the Feynman amplitude for the collision is

$$M = g^6 \frac{2p \cdot \tilde{a}_1 2p \cdot \tilde{a}_2 2p \cdot \tilde{a}_3}{2m^5 q_1^2 q_2^2 q_3^2} T_a^{(1)} T_b^{(2)} T_c^{(3)} \\ \times \left\{ T_a T_b T_c M_{123} + T_a T_c T_b M_{132} + T_b T_c T_a M_{231} \right. \\ \left. + T_b T_a T_c M_{213} + T_c T_a T_b M_{312} + T_c T_b T_a M_{321} \right\} \quad (53)$$

where $T_{a,b,c}$ without a superscript are the color matrices for the incident quark jet p , and the amplitudes $M_{123}, M_{132}, M_{231}, M_{213}, M_{312}, M_{321}$ are sequentially the six terms in the curly brackets of the Abelian Feynman amplitude components in Eq. (16). It is easy to show that the quantity in the curly bracket of Eq. (53) can be re-written as

$$\mathcal{M} = \{T_a [T_b T_c]_+ + T_b [T_c T_a]_+ + T_c [T_a T_b]_+\} \\ \times [M_{123} + M_{132} + M_{231} + M_{213} + M_{312} + M_{321}]/2 \\ - T_a [T_b T_c]_- [M_{231} + M_{213} + M_{312} + M_{321}]/2 \\ - T_b [T_c T_a]_- [M_{123} + M_{132} + M_{312} + M_{321}]/2 \\ - T_c [T_a T_b]_- [M_{123} + M_{132} + M_{231} + M_{213}]/2 \\ + T_a [T_b T_c]_- (M_{123} - M_{132})/2 \\ + T_b [T_c T_a]_- (M_{231} - M_{213})/2 \\ + T_c [T_a T_b]_- (M_{312} - M_{321})/2. \quad (54)$$

The first term on the right hand side involves the symmetric sum of the space-time part of permuted amplitudes as in the Abelian case, multiplied by the symmetric permutation of the color indices. It yields a Feynman amplitude that is just the Abelian Feynman amplitude multiplied by the color factor

$$T_a^{(1)} T_b^{(2)} T_c^{(3)} \{T_a [T_b T_c]_+ + T_b [T_c T_a]_+ + T_c [T_a T_b]_+\} / 2 \quad (55)$$

The other terms involve partial symmetry and antisymmetry with respect to the exchange of color indices. Similar studies on the collision of a jet with n partons can

be carried out as in [71–78]. For our present work, it suffices to note that there will always be a component of the Feynman amplitude that is symmetric under both space-time exchange and color index exchange involving the sum of all space-time amplitude components, similar to the $\mathcal{M}_1 + \mathcal{M}_2$ sum in Eq. (50) and the first term on the right-hand side of Eq. (54). There will also be other space-time antisymmetric and color index exchange antisymmetric components.

For the space-time symmetric and color index exchange symmetric component, the Feynman amplitude is equal to the Abelian Feynman amplitude multiplied by a color factor. It will exhibit the same degree of Bose-Einstein interference as in the Abelian theory. Previous analysis on the longitudinal momentum transfer of recoiling fermions in the Abelian theory in Section 2 can be applied for the non-Abelian theory for this space-time symmetric and color index exchange symmetric component. There is thus a finite probability for the presence of delta function constraints to lead to recoiling quarks receiving significant moment kicks along the direction of the incident quark jet.

V. COLLISION OF A GLUON JET WITH QUARK SCATTERERS

It is of interest to generalize the above considerations to the coherent multiple collisions of a gluon jet. We shall neglect four-particle vertices and loops, which are of higher-orders. The Feynman diagrams for the collision of a gluon jet with medium quarks or medium gluons then have structures and momentum flows the same as those in the collision of a quark jet with quark scatterers. In the high-energy limit, the propagators and the three-particle vertices have approximately the same momentum dependencies, and the Bose-Einstein symmetry with respect to the interchange of the virtual bosons is the same. One expects that aside from the presence of color factors and color indices, the results for the Bose-Einstein interference in collisions with a gluon jet or a quark jet should be similar. This is so because the high-energy processes are insensitive to the spins of the colliding particles, as the current carried by a high energy particle is dominated by its center-of-mass motion, much more so than its spin current [74, 79, 80].

It is instructive to study the coherent collision of a fast gluon with two quarks in non-Abelian gauge field theories in the reaction $p + a_1 + a_2 \rightarrow p' + a'_1 + a'_2$ as an examples of the type of BE interference for the collision of a gluon jet. The collision process is represented by the two Feynman diagrams in Fig. 4.

We consider the Feynman amplitude matrix element between the initial three particle state $|pa\alpha, a_1f\phi, a_2k\kappa\rangle$ and the final state $|p'c\gamma, a'_1h\eta, a'_2l\lambda\rangle$ where $\{a, f, k, c, h, l\}$ label the color states and $\{\alpha, \phi, \kappa, \gamma, \eta, \lambda\}$ label components of various particle currents. Using the Feynman rules and the overall phase factors as given in Ref. [72],

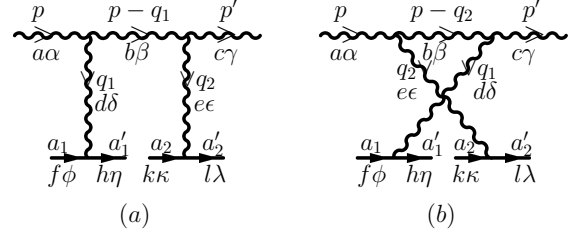


FIG. 4: Feynman diagrams for the collision of a gluon jet p with quark partons a_1, a_2 with the momentum transfer q_1 and q_2 in the reaction $p + a_1 + a_2 \rightarrow p' + a'_1 + a'_2$. Here, $\{a, b, c, \dots, k, l\}$ label the color states and $\{\alpha, \beta, \dots, \eta, \lambda\}$ label the momentum components of various particles.

the Feynman amplitude matrix element of Fig. 4(a) is given by

$$\begin{aligned} & \langle p'c\gamma, a'_1h\eta, a'_2l\lambda | M_1 | pa\alpha, a_1f\phi, a_2k\kappa \rangle \\ &= g^4 \frac{f_{bec}f_{bad}}{q_1^2 q_2^2 (2p \cdot q_1 - i\epsilon)} (T_e^{(2)})_{lk} (T_d^{(1)})_{hf} \epsilon_\gamma(p') \\ & \times \{g_{\gamma\beta}(p' + p - q_1)_\epsilon + g_{\beta\epsilon}(-p + q_1 - q_2)_\gamma + g_{\epsilon\gamma}(q_2 - p')_\beta\} \\ & \times \{g_{\beta\alpha}(2p - q_1)_\delta + g_{\alpha\delta}(-p - q_1)_\beta + g_{\delta\beta}(2q_1 - p)_\alpha\} \epsilon_\alpha^*(p) \\ & \times \bar{u}(a'_2)\gamma_\epsilon u(a_2)\bar{u}(a'_1)\gamma_\delta u(a_1), \end{aligned} \quad (56)$$

where $\epsilon(p)$ and $\epsilon(p')$ are the polarization vectors for gluons p or p' respectively. In the high-energy limit in which $|p| \gg \{|q_i|, |a_i|, m\}$, terms of order $\{|q_i|/|p|, |a_i|/|p|, m/|p|\}$ in the three-gluon vertices can be neglected, and the helicities can be assumed to conserve. We then obtain

$$\begin{aligned} & \langle p'c\gamma, a'_1h\eta, a'_2l\lambda | M_1 | pa\alpha, a_1f\phi, a_2k\kappa \rangle \\ &= -\frac{g^4 (T_e^{(p)})_{cb} (T_d^{(p)})_{ba} (T_e^{(2)})_{lk} (T_d^{(1)})_{hf}}{q_1^2 q_2^2 (2p \cdot q_1 - i\epsilon)} \frac{2p \cdot \tilde{a}_1}{m} \frac{2p \cdot \tilde{a}_2}{m}, \end{aligned} \quad (57)$$

where the coefficients f_{bec} and f_{bad} in Eq. (56) have been expressed as matrix elements of matrices $T_d^{(p)}$ and $T_e^{(p)}$ of the incident gluon p (or p') between gluon color states [72],

$$(T_d^{(p)})_{ba} = if_{dba}, \quad (58)$$

$$(T_e^{(p)})_{cb} = if_{ecb}. \quad (59)$$

Equation (57) can be re-written in a matrix form as

$$M_1 = -g^4 \frac{2p \cdot \tilde{a}_1 2p \cdot \tilde{a}_2}{m^2 q_1^2 q_2^2} \frac{T_e^{(p)} T_d^{(p)} T_e^{(2)} T_d^{(1)}}{2p \cdot q_1 - i\epsilon}. \quad (60)$$

We can obtain a similar result for the Feynman amplitude for diagram 4(b) by permuting the vertices of the exchange bosons. As a consequence, the sum of the two Feynman amplitudes from Figs. 4(a) and 4(b) is given by

$$\begin{aligned} M &= -g^4 \frac{2p \cdot \tilde{a}_1 2p \cdot \tilde{a}_2}{m^2 q_1^2 q_2^2} \\ & \times \left\{ \frac{T_e^{(p)} T_d^{(p)} T_e^{(2)} T_d^{(1)}}{2p \cdot q_1 - i\epsilon} + \frac{T_d^{(p)} T_e^{(p)} T_e^{(2)} T_d^{(1)}}{2p \cdot q_2 - i\epsilon} \right\}. \end{aligned} \quad (61)$$

We note that the above equation for the collision of a gluon jet is in the same form as Eq. (45) for the collision of a quark jet except with the modification that in the above equation for a gluon jet, the operator $T^{(p)}$ has matrix elements between gluon color states whereas the operator $T^{(p)}$ in Eq. (45) for the quark jet has matrix elements between quark color states. As in Eq. (45), we can likewise express the product of the color matrices as

$$T_b^{(p)} T_a^{(p)} = \frac{1}{2} \left([T_b^{(p)}, T_a^{(p)}]_+ + [T_b^{(p)}, T_a^{(p)}]_- \right), \quad (62)$$

$$T_a^{(p)} T_b^{(p)} = \frac{1}{2} \left([T_b^{(p)}, T_a^{(p)}]_+ - [T_b^{(p)}, T_a^{(p)}]_- \right). \quad (63)$$

The Feynman amplitude for a gluon jet is then

$$M \sim -g^4 \frac{2p \cdot \bar{a}_1 2p \cdot \bar{a}_2}{2m^3 q_1^2 q_2^2} \left\{ (\mathcal{M}_1 + \mathcal{M}_2) \frac{[T_b^{(p)}, T_a^{(p)}]_+ T_b^{(2)} T_a^{(1)}}{2} + (\mathcal{M}_1 - \mathcal{M}_2) \frac{[T_b^{(p)}, T_a^{(p)}]_- T_b^{(2)} T_a^{(1)}}{2} \right\}. \quad (64)$$

Therefore, in the collision of both a gluon or a quark jet with quarks, there will always be a component of the Feynman amplitude that is symmetric under both space-time exchange and color index exchange, involving the sum of all space-time amplitude components. The similarity is so close that previous results concerning a quark jet in collision with quark scatterers apply equally well to a gluon jet.

VI. COLLISION OF A GLUON JET WITH GLUON SCATTERERS

There is however a small difference in the coherent collisions of a jet with gluon scatterers. We can consider the collision of a fast gluon p with two gluon scatterers a_1 and a_2 as shown in Fig. 5.

The matrix element of the Feynman amplitude in Fig. 4(a) is given by

$$\begin{aligned} & \langle p' c \gamma, a'_1 h \eta, a'_2 l \lambda | M_1 | p a \alpha, a_1 f \phi, a_2 k \kappa \rangle \\ &= -\frac{g^4 f_{bec} f_{bad} f_{kle} f_{fhd}}{q_1^2 q_2^2 (2p \cdot q_1 - i\epsilon)} \epsilon_\gamma(p') \epsilon_\alpha^*(p) \epsilon_\lambda(a'_2) \epsilon_\kappa^*(a_2) \epsilon_\eta(a'_1) \epsilon_\phi^*(a_1) \\ & \times \{ g_{\gamma\beta}(p' + p - q_1)_\epsilon + g_{\beta\epsilon}(-p + q_1 - q_2)_\gamma + g_{\epsilon\gamma}(q_2 - p')_\beta \} \\ & \times \{ g_{\beta\alpha}(2p - q_1)_\delta + g_{\alpha\delta}(-p - q_1)_\beta + g_{\delta\beta}(2q_1 - p)_\alpha \} \\ & \times \{ g_{\kappa\lambda}(-a_2 - a'_2)_\epsilon + g_{\lambda\epsilon}(a'_2 + q_2)_\kappa + g_{\epsilon\kappa}(-q_2 + a_2)_\lambda \} \\ & \times \{ g_{\phi\eta}(-a_1 - a'_1)_\delta + g_{\eta\delta}(a'_1 + q_1)_\phi + g_{\delta\phi}(-q_1 + a_1)_\eta \}. \end{aligned} \quad (65)$$

In the high-energy limit in which $|\mathbf{p}| \gg \{|\mathbf{q}_i|, |\mathbf{a}_i|, m\}$ and the helicities can be assumed to conserve, we obtain

$$\begin{aligned} & \langle p' c \gamma, a'_1 h \eta, a'_2 l \lambda | M_1 | p a \alpha, a_1 f \phi, a_2 k \kappa \rangle \\ &= -\frac{4g^4 (T_e^{(p)})_{cb} (T_d^{(p)})_{ba} (T_e^{(2)})_{lk} (T_d^{(1)})_{hf}}{q_1^2 q_2^2 (2p \cdot q_1 - i\epsilon)} 2p \cdot \bar{a}_1 2p \cdot \bar{a}_2 \end{aligned} \quad (66)$$

where

$$\bar{a}_i = \frac{a_i + a'_i}{2}. \quad (67)$$

We can obtain a similar result for the Feynman amplitude for diagram 5(b) by permuting the vertices of the exchange bosons. As a consequence, the sum of the two Feynman amplitudes from Figs. 5(a) and 5(b) is given by

$$M = -4g^4 \frac{2p \cdot \bar{a}_1 2p \cdot \bar{a}_2}{q_1^2 q_2^2} \times \left\{ \frac{T_e^{(p)} T_d^{(p)} T_e^{(2)} T_d^{(1)}}{2p \cdot q_1 - i\epsilon} + \frac{T_d^{(p)} T_e^{(p)} T_e^{(2)} T_d^{(1)}}{2p \cdot q_2 - i\epsilon} \right\}. \quad (68)$$

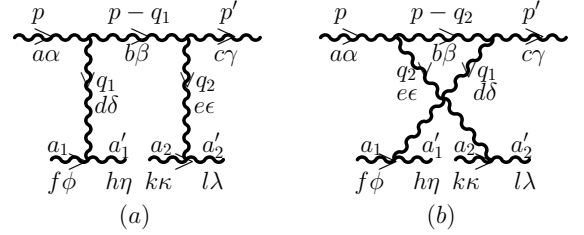


FIG. 5: Feynman diagrams for the interaction of a gluon jet p with gluon scatterers a_1, a_2 with the momentum transfer q_1 and q_2 . Here, $\{a, b, c, \dots, k, l\}$ label the color states and $\{\alpha, \beta, \dots, \eta, \lambda\}$ label the momentum components of various particles.

By comparing the results for a quark jet on quark scatterers [Eq. (45)] with those for a gluon jet on quark scatterers [Eq. 61] or on gluon scatterers [Eq. (68)], we obtain the following simple rules to obtain from the results of quark jet on quark scatterers of Eq. (45) to those involving gluons: (1) provide an overall multiplicative factor of $2m$ when a quark is replaced by a gluon, (2) keep the same form of the color operators, with the color operators that operate on the quark color states switched to operate on the gluon color states, and (3) change the momentum variable \tilde{a}_i of Eq. (4) for a quark scatterer to \bar{a}_i of Eq. (67) for a gluon scatterer when a quark scatterer is replaced by a gluon scatterer. The above Rule (1) and (2) are well known results that were obtained previously on page 198 of Ref. [72]. Rule (3) is for our case in the collision with many scatterers.

For completeness, we can use these rules to obtain the Feynman amplitude for the collision of a quark jet with two gluon scatterers as

$$M = -2g^4 \frac{2p \cdot \bar{a}_1 2p \cdot \bar{a}_2}{m q_1^2 q_2^2} \times \left\{ \frac{T_e^{(p)} T_d^{(p)} T_e^{(2)} T_d^{(1)}}{2p \cdot q_1 - i\epsilon} + \frac{T_d^{(p)} T_e^{(p)} T_e^{(2)} T_d^{(1)}}{2p \cdot q_2 - i\epsilon} \right\}. \quad (69)$$

VII. LONGITUDINAL MOMENTUM TRANSFER FOR GLUONS SCATTERERS

The results in the last section indicate that there is a modification from \tilde{a} of Eq. (4) for a quark scatterer to \bar{a}_i of Eq. (67) for a gluon scatterer when a quark scatterer is replaced by a gluon scatterer. Such a modification brings with it a change in the longitudinal momentum distribution of the gluon scatterers which we shall examine in this section.

We consider the coherent multiple collisions of a quark jet or a gluon jet on n gluons scatterers. From the results in Eq. (25), the cross section for the scattering in the space-time symmetric and color symmetric state is proportional to

$$d\sigma \propto \delta(p'_0 + \sum_{i=1}^n q_{i0} - p_0) \frac{1}{p'_0} \prod_{i=1}^n \frac{(2p \cdot \bar{a}_i)^2 dq_{iz} d\mathbf{q}_{iT}}{2a'_{i0} |\mathbf{q}_{iT}|^4}. \quad (70)$$

The reaction has high probabilities for the occurrence of small values of $|\mathbf{q}_{iT}|$. To investigate the longitudinal distribution of the scatterers, we need to investigate the q_{iz} dependence of the factor $(2p \cdot \bar{a}_i)^2$ in Eq. (70), which can be written as

$$(2p \cdot \bar{a}_i)^2 = [2p \cdot (2a_i + q_i)]^2. \quad (71)$$

Because of the $\Delta(2p \cdot q_i)$ constraint, the above factor becomes

$$(4p \cdot a_i)^2, \quad (72)$$

that is independent of q_{iz} of the scatterers. It is con-

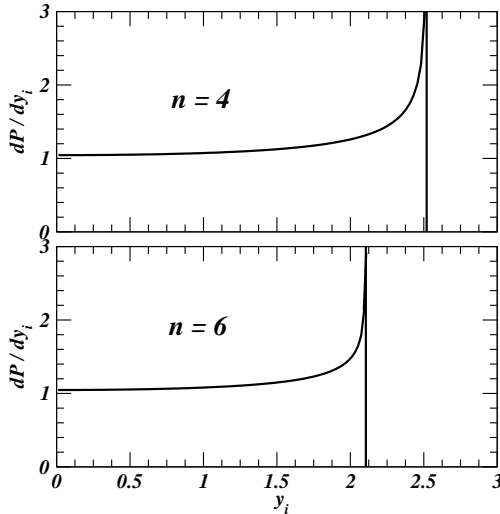


FIG. 6: The average dP/dy_i for the rapidity of the gluon scatterer in the collision of a fast jet $p_0 = 10$ GeV with $n=4$ and 6 gluons of gluon transverse mass $m_{gT} = 0.4$ GeV.

venient to use the rapidity variable y_i to represent the longitudinal momentum transfer q_{iz} ,

$$q_{iz} = m_{gT} \sinh y_i, \quad (73)$$

$$a'_{i0} = \sqrt{m_{gT}^2 + (a_{iz} + m_{gT} \sinh y_i)^2}, \quad (74)$$

where for simplicity the final transverse masses of the scatterers are taken to be their average value m_{gT} . To make the problem simple, we can take a_{iz} to have its average value $\langle a_{iz} \rangle$, which is zero in the medium center-of-momentum frame. From Eq. (70), the unnormalized probability distribution for the y_i variables of the gluon scatterers becomes

$$\frac{dP}{dy_1 dy_2 \dots dy_n} = \frac{1}{(p_0 - a'_{10} - a'_{20} - \dots - a'_{n0})}, \quad (75)$$

which differs from the distribution in Eq. (37) for quark scatterers. On average, the rapidities y_i for different scatterers are approximately the same. As far as y_i is concerned, the unnormalized distribution on the average is

$$\left. \frac{dP}{dy_i} \right|_{y_j=y_i, j=1, \dots, n} \sim \frac{1}{(1 - nm_{gT} \cosh y_i/p_0)^{1/n}}. \quad (76)$$

In Fig. 6, we plot this “average” dP/dy_i as a function of y_i for the case of $n = 4$ and 6 with $p_0 = 10$ GeV/c, and $m_{gT} = 0.4$ GeV. The probability distribution is nearly flat for most of the allowed regions and rises rapidly as y_i approaches the limit

$$y_{i\max} = \cosh^{-1} \left\{ \frac{1}{p_0/nm_{gT}} \right\}. \quad (77)$$

The above estimate (76) is based on the assumption that in the high-energy limit, p' is not significantly different from p . It may not be applicable in the regions of y_i close to $y_{i\max}$ for which p' is substantially reduced from p . Therefore, the estimate of $\langle y_i \rangle$ obtained with (76) can only be considered as an upper limit. On the other hand, the probability distribution is relatively flat for small values of y_i and it increases monotonically as y_i increases near $y_{i\max}$. If the probability distribution dP/dy_i were flat as a function of y_i , the average $\langle p'_{iz} \rangle$ would be

$$\langle q_{iz} \rangle = \frac{p_0/n - m_{gT}}{y_{i\max}}. \quad (78)$$

which should be the lower limit of $\langle p'_{iz} \rangle$. The upper limit is then given by the distribution (76) by numerical integration. With $p_0 = 10$ GeV/c and $m_{gT} = 0.4$ GeV, we find for $n = 6$,

$$0.6 \text{ GeV/c} \lesssim \langle q_{iz} \rangle \lesssim 0.66 \text{ GeV/c}, \quad (79)$$

and for $n = 4$, we find

$$1.3 \text{ GeV/c} \lesssim \langle q_{iz} \rangle \lesssim 1.62 \text{ GeV/c} \quad (80)$$

These estimates indicate that the average longitudinal momentum kick acquired by a gluon scatterer is slightly smaller than that acquired by a fermion scatterer. They are approximately inversely proportional to the number of scatterers in a coherent collision.

VIII. SIGNATURES OF BOSE-EINSTEIN INTERFERENCE AND COMPARISON WITH EXPERIMENTAL DATA

The results in the above sections provide information on the signatures for the occurrence of the Bose-Einstein interference in the coherent collisions of a jet with medium partons:

1. The Bose-Einstein interference is a quantum many-body effect. It occurs only in the multiple collisions of the fast jet with two or more scatterers. Therefore there is a sharp threshold corresponding to the requirement of two or more scatterers in the multiple collisions, $n \geq 2$.
2. Each scatterer has a transverse momentum distribution of the type $1/|q_T|^4$, which peaks at small values of $|q_T|$.
3. Each scatterer acquires a longitudinal momentum kick along the incident jet direction that is approximately inversely proportional to the number of scatterers.
4. As a consequence, the final effect is the occurrence of collective recoils of the scatterers along the jet direction.

To inquire whether Bose-Einstein interference may correspond to any observable physical phenomenon, it is necessary to identify the scatterers to separate them from the incident jet in a measurement. Such a separation is indeed possible in $\Delta\phi$ - $\Delta\eta$ angular correlation measurements of produced pairs with a high- p_T trigger [1]-[23]. Particles in the “ridge” part of the correlations with $|\Delta\eta| > 0.6$ and $\Delta\phi \sim 0$ can be identified as belonging to the medium partons because

1. The yield of these ridge particles increases approximately linearly with the number of participants [3].
2. The yield of these ridge particles is nearly independent of (i) the flavor content, (ii) the meson/hyperon character, and (iii) the transverse momentum p_T (above 4 GeV) of the jet trigger [3, 4, 6].
3. The ridge particles have a temperature (inverse slope) that is similar (but slightly higher) than that of the inclusive bulk particles, but lower than the temperature of the near-side jet fragments [3].
4. The baryon/meson ratio of these ridge particles is similar to those of the bulk hadrons and is quite different from those in the jet fragments [19].

With the scatterers as ridge particles that can be separated from the incident high- p_T jet, the occurrence of the Bose-Einstein interference will be signaled by the collective recoils of the scatterers (the ridge particles) along the jet direction. The collective recoils will lead to the

$\Delta\phi \sim 0$ correlation of the ridge particles with the high- p_T trigger, as has been observed in angular correlations of produced hadrons in AuAu collisions at RHIC [1]-[23]. The collective recoils of the kicked medium partons have been encoded into the longitudinal momentum kick $\langle q_{iz} \rangle$ of the momentum kick model that yields the observed $\Delta\phi$, $\Delta\eta$, and p_T dependencies of the angular correlations [28-35].

It is of interest to examine item (3) of the signature of the Bose-Einstein interference with regarding to the relationship between the (average) magnitude of the longitudinal momentum kick, $\langle q_{iz} \rangle$, and the (average) number of scatterers, $\langle n \rangle$, when such a collective momentum kick occurs. For the most central AuAu collisions at $\sqrt{s_{NN}} = 200$ GeV at RHIC, we previously found that $\langle f_R \rangle \langle n \rangle \sim 3.8$ where n is the number of kicked medium partons and $\langle f_R \rangle$ is the average attenuation factor for the kicked partons to emerge from the collision zone [30]. The value of $\langle f_R \rangle$ is not determined but a similar attenuation factor $\langle f_J \rangle$ for jet fragments is of order 0.63 [30]. We can therefore estimate that for the most central AuAu collisions at $\sqrt{s_{NN}} = 200$ GeV at RHIC, $\langle n \rangle \sim 6$. For an incident jet of $p_z \sim 10$ GeV/c [20] and a momentum cut-off of $\Lambda_{\text{cut}} = 0.3$ GeV/c, the estimate of Eq. (42) gives the range of the average longitudinal momentum kick for quark scatterers,

$$0.83 \text{ GeV/c} \lesssim \langle q_{iz} \rangle \lesssim 0.91 \text{ GeV/c}, \quad (81)$$

and the estimate of Eq. (79) gives the average longitudinal momentum kick for gluon scatterers. These estimates of the momentum kick are of the same order as the value of $\langle q_{iz} \rangle \sim 1$ GeV/c estimated in [30] and 0.8 GeV/c in [32], obtained in the momentum kick model analysis.

In another momentum kick model analysis for the highest multiplicity pp collisions at $\sqrt{s_{NN}} = 7$ TeV at the LHC, we previously found that $\langle f_R \rangle \langle n \rangle \sim 1.5$ [35] and we can estimate $\langle n \rangle \sim 2.4$. The estimate of Eq. (42) gives the range of the average longitudinal momentum kick of quark scatterers for an incident jet of 10 GeV/c as

$$2.1 \text{ GeV/c} \lesssim \langle q_{iz} \rangle \lesssim 2.6 \text{ GeV/c}, \quad (82)$$

and the estimate of Eq. (80) gives the average longitudinal momentum kick of gluon scatterers. These estimates of the momentum kick are of the same order as the value of $\langle q_{iz} \rangle \sim 2$ GeV/c estimated in [35] in the momentum kick model. The experimental data give a longitudinal momentum transfer that is approximately inverse proportional to the number of scatterers.

With regard to item (1) for the signature for the occurrence of the Bose-Einstein interference, the presence of a threshold implies a sudden increase of the ridge yield as a function of centrality, as represented by the number of participants. We show in Fig. 7 the experimental ridge yield per high- p_T trigger as a function of N_{part} for AuAu and CuCu collisions at $\sqrt{s} = 200$ and 62 GeV at RHIC [4, 10]. We also show in Fig. 7 the theoretical yields

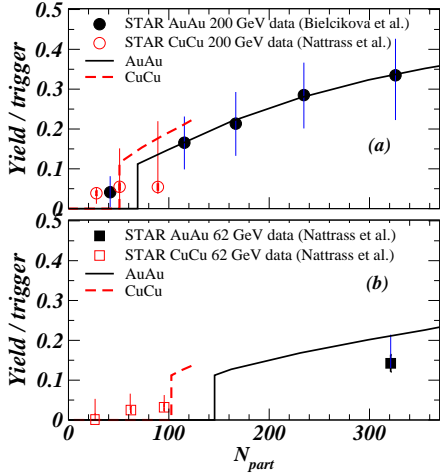


FIG. 7: (Color online) The ridge yield per high- p_T trigger as a function of the participant number N_{part} for nucleus-nucleus collisions at $\sqrt{s_{NN}}=200$ and 62 GeV. The solid circular points (for AuAu) and the square points (for CuCu) are from the STAR Collaboration [4, 10]. The curves are the momentum kick model results of [31] modified to include the Bose-Einstein interference threshold effect of $n \geq 2$.

obtained in the momentum kick model [30], where the ridge yield at the most central collision at $N_{\text{part}} = 320$ was calibrated as $n = 6$ [30]. With such a calibration, the threshold values in N_{part} at which $n = 2$ can be located and listed in Table I, where the 30% theoretical errors arise from the errors in measuring the ridge yield at the most central collision at $N_{\text{part}} = 320$. Theoretical ridge yields from the momentum kick analysis in Fig. 10 of Ref. [30], modified to include the Bose-Einstein interference threshold effect of $n \geq 2$, are shown as the solid curves for AuAu collisions, and as dashed curves for CuCu collisions in Fig. 7. The sharp theoretical thresholds in Fig. 7 will be smoothed out by the uncertainties in the estimates of the number of scatterers and the fluctuations of the number of scatterers as a function of N_{part} . Although the experimental data appear to be consistent with theory and with the presence of thresholds, the large error bars and the scarcity of the number of data points in the threshold regions preclude a definitive conclusion.

However, as shown in Fig. 8, sharp threshold effects for the ridge yield (2D Gaussian yield) as a function of N_{part} have been observed in another angular correlation measurements with a low- p_T trigger from the STAR Collaboration [14–17]. We note previously that a fast jet parton possesses low- p_T jet fragments and a minimum- p_T -biased low- p_T trigger can also indicate the passage of a fast parent jet [35]. As a consequence, ridge particles will also be associated with a low- p_T trigger. The ridge yield will increase with N_{part} , as N_{part} increases with the number of (parent jet)-(medium parton) collisions, which gives the number of kicked medium partons and the ridge yield [31]. The sudden increase of the amplitude and the peak η width of the ridge yield as a function of N_{part} , as

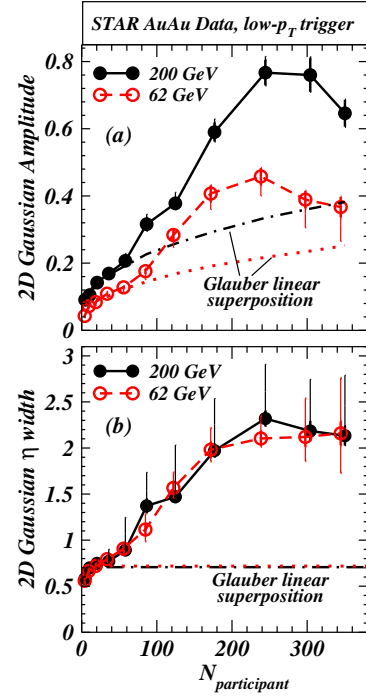


FIG. 8: (Color online) STAR Collaboration data of (a) the peak amplitude and (b) the peak η width of the 2D Gaussian (ridge yield) as a function of N_{part} , for AuAu collisions at $\sqrt{s_{NN}}=200$ GeV (solid circles) and 62 GeV (open circles), with a low- p_T trigger [14–17]. The solid and dashed curves are lines joining the data points. The dashed-dot and dotted curves represent Glauber linear superposition (GLS) estimates.

shown in Fig. 8(a) and 8(b), indicates the presence of a threshold for the ridge yield as a function of centrality.

TABLE I: (Color online) Comparison of the locations of the theoretical threshold, at which the (average) number of scatterer n is equal to 2, with the observed experimental threshold [14–17] for the sudden increase of the peak amplitude and width of the 2D Gaussian component (ridge component) in AuAu collisions at $\sqrt{s_{NN}} = 200$ and 62 GeV in Fig. 8.

Collision System	$\sqrt{s_{NN}}$ (GeV)	Theoretical Threshold N_{part}	Experimental Threshold N_{part}
AuAu	200	69 ± 21	58-86
AuAu	62	146 ± 45	85-122
CuCu	200	51 ± 15	
CuCu	62	103 ± 31	

For AuAu at 200 GeV/c, the experimental ridge yield threshold occurs at $N_{\text{part}} = 58 - 86$ (Fig. 8), which can be compared in Table I with the theoretical ridge yield threshold of $N_{\text{part}} = 69 \pm 21$ as estimated in the momentum kick model for $n = 2$. For AuAu at 62 GeV/c, the experimental ridge yield threshold occurs at $N_{\text{part}} = 85 - 122$ (Fig. 8), which can be compared with the theoretical threshold of $N_{\text{part}} = 146 \pm 45$ as estimated in the momentum kick model for $n = 2$ (Table I).

These comparisons indicate that experimental data with low- p_T trigger are consistent with the presence of ridge thresholds as a function of the number of the medium scatterers located at $n \sim 2$, as in the threshold effect in Bose-Einstein interference.

IX. CONCLUSIONS AND DISCUSSIONS

Stimulated by the phenomenological successes of the momentum kick model in the analysis of the angular correlations of hadrons produced in high-energy heavy-ion collisions [28–35], we seek a theoretical foundation for the origin of the longitudinal momentum kick postulated in the model. We explore whether such a longitudinal momentum kick may originate from a quantum many-body effect arising from the Bose-Einstein interference in the passage of a jet in a dense medium. We take note of previous results on the Bose-Einstein interference in the emission of real photons and gluons in high-energy interactions and in the sum of the ladder and cross-ladder loop diagrams in the collision of two particles [71–78].

We find similarly that in the coherent collisions of an energetic fermion with n fermion scatterers at high energies in the Abelian theory, the symmetrization of the scattering amplitude with respect to the interchange of the virtual bosons leads to the Bose-Einstein interference, resulting in sharp distributions at $p \cdot q_i \sim 0$. Such coherent collisions are in fact a single collision, tying the incident fermion with the n fermion scatterers as a single unit. There are then $3(n+1)$ degrees of freedom, which are reduced to $3n-1$ degrees after taking into account the constraints of the conservation of energy and momentum. As a consequence, all $3n$ degrees of freedom of the scatterers can be independently varied, subject only to a single condition of the overall conservation of energy. The probability distribution in these $3n$ degrees of freedom depends on the phase-space factors and the functional dependence of the Feynman amplitude matrix element. The Bose-Einstein symmetry constraints of $p \cdot q_i \sim 0$ limit the transverse momentum transfers of the scatterers to small values of q_{iT} . The longitudinal momenta of the scatterers get their share of longitudinal momenta from the jet, resulting in the collective recoils of the scatterers along the jet direction.

For the coherent collision of an energetic parton with parton scatterers in non-Abelian cases, we find that the complete Bose-Einstein symmetry in the exchange of virtual gluons consists not only of space-time exchange symmetry but also color index exchange symmetry. Nevertheless, there is always a space-time symmetric and color-index symmetric component of the Feynman amplitude that behaves the same way as the Feynman amplitude in the Abelian case, in addition to the occurrence of space-time antisymmetric and color-index antisymmetric components. For the space-time symmetric and color-index symmetric component, the recoiling partons behave in the same way as in collisions in the Abelian case. There

is thus a finite probability for the parton scatterers to emerge collectively along the incident trigger jet direction, each with a significant fraction of the longitudinal momentum of the incident jet. The collective recoils will lead to the $\Delta\phi \sim 0$ correlation of the ridge particles with the high- p_T trigger. Such a signature of the Bose-Einstein interference has probably been observed in the $\Delta\phi \sim 0$ correlation of the ridge particles with a high- p_T trigger in the angular correlation measurements of produced hadron pairs in AuAu collisions at RHIC [1]–[23]. The centrality dependence of the ridge yield in AuAu collisions at $\sqrt{s_{NN}} = 200$ GeV with a low- p_T trigger [14–17] is also consistent with the presence of a ridge threshold at $n = 2$, as expected in the quantum many-body effect of Bose-Einstein interference.

The present work is based on the high-energy limit which allows great simplifications of the algebraic structures of Feynman amplitude components. These simplified structures bring into clear focus the mechanism of the Bose-Einstein interference that changes the nature of the distribution function. With the mechanism of the Bose-Einstein interference well understood, it may be beneficial in future work to evaluate the Feynman amplitudes without resorting to many of the drastic assumptions and simplifications – in order to make quantitative comparison of theoretical predictions with results of the longitudinal momentum kick quantities extracted from experimental data. This is particularly important in regions of large longitudinal momentum transfers for which the high-energy approximation of having p' not greatly different from p may not hold.

Many models have been proposed to explain the ridge phenomenon [28–70]. They include the collision of jets with medium partons [28–35, 56, 57], flows and hydrodynamics with initial state fluctuations [36, 37, 44, 45, 53, 55, 62], color-glass condensate [43–45, 49, 54], modeling pQCD [58–61], parton cascade [63], gluon bremsstrahlung in string formation [64], strong-coupling AdS/CFT [66], quantum entanglement [68], and BFKL evolution and beyond [70]. There are however two difficulties associated with these phenomenological models. Almost all models deal with fragmented parts of the data and all models contain implicit and explicit assumptions.

In the presence of a large number of models and the above difficulties, progress can proceed in three fronts. First, the models need to cover an extensive set of experimental differential data over large phase spaces, centralities, and energies, from many different collaborations. Secondly, the assumptions of the models need further theoretical and observational investigations from fundamental viewpoints. Finally, experimental tests need to be proposed to distinguish different models.

With regard to the first of these three tasks, the momentum kick model gives reasonable descriptions for an extensive set of differential data of the ridge yield, over an extended range of transverse momenta, azimuthal angles, pseudorapidity angles, centralities, and collision energies, from the STAR Collaboration [1–5], the PHENIX

Collaboration [20–23], the PHOBOS Collaboration [25], and the CMS Collaboration [26]. In these momentum kick model analyses, a collective longitudinal momentum kick on the medium scatterers along the jet direction is a central ingredient leading to the successful descriptions of the large set of experimental data. Additional analyses will be continued to extend the momentum kick model to include the effects of collective flows and to cover a larger set of new data as they become available.

With regard to the second of the three tasks, the momentum kick model contains the basic assumption that the $\Delta\eta$ ridge arises mainly from the initial rapidity distribution of partons prior to the jet collision. Such a basic assumption has been examined from the viewpoint of the Wigner function of produced particles in a fundamental quantum theory of particle production [33]. Another basic assumption concerning the longitudinal nature of the momentum kick is now being examined in the present manuscript.

With regard to third of the three tasks, the present analysis for jets interacting with medium partons reveals that the longitudinal momentum kick is a quantum many-body effect that contains a threshold, requiring the multiple collisions of the jet with at least two partons. This is in agreement with the sudden onset of the ridge yield as a function of the centrality, observed by the STAR Collaboration [2, 14–18], as discussed in Section VIII. Furthermore, in the momentum kick model with longitudinal momentum kicks, the kicked medium partons from back-to-back jets possess a (p_{1T}, p_{2T}) correlation for both the near side and the away side, as observed by the STAR Collaboration [18, 35].

It would be of interest to see how other proposed models fare with the three tasks at hand. It will also be of interest to see whether they contain the features of a sudden onset of the ridge yield as a function of the centrality,

and the (p_{1T}, p_{2T}) correlation for both the near side and the away side. The search for tests to distinguish different models will be an on-going research activity.

Whatever the theoretical descriptions, minijets of order 10 GeV and below are known to be present in high-energy collisions [20–24, 81]. These minijets collide with medium partons. They are not hydrodynamical flows, but they contribute to the azimuthal anisotropy and the azimuthal Fourier coefficients [82–84], as well as to two-particle correlations. They must be taken into account or be subtracted from experimental data in theoretical models that do not include the minijet effects explicitly.

In summary, Bose-Einstein interference in the passage of a jet in a dense medium is a quantum many-body effect that occurs quite generally in a coherent multiple collision process, with the threshold of more than two scatterers. The manifestation of the Bose-Einstein interference effect as collective recoils of the scatterers along the jet direction may have been experimentally observed in the angular correlation of hadrons associated with a high- p_T trigger in high-energy AuAu collisions at RHIC. In angular correlation measurements of the same reaction with a low- p_T trigger, the experimental observation of a ridge threshold as a function of centrality lends additional support for the occurrence of the Bose-Einstein interference threshold in the passage of a jet in a dense medium.

Acknowledgment

The author wishes to thank Profs. C. S. Lam, H. W. Crater, Jin-Hee Yoon, Vince Cianciolo, and A. V. Koshelkin for helpful discussions. This research was supported in part by the Division of Nuclear Physics, U.S. Department of Energy.

-
- [1] J. Adams *et al.* for the STAR Collaboration, Phys. Rev. Lett. **95**, 152301 (2005);
 - [2] J. Adams *et al.* (STAR Collaboration), Phys. Rev. C **73**, 064907 (2006).
 - [3] J. Putschke (STAR Collaboration), J. Phys. **G34**, S679 (2007).
 - [4] J. Bielcikova (STAR Collaboration), J. Phys. **G34**, S929 (2007).
 - [5] F. Wang (STAR Collaboration), Invited talk at the XIth International Workshop on Correlation and Fluctuation in Multiparticle Production, Hangzhou, China, November 2007, [arXiv:0707.0815].
 - [6] J. Bielcikova (STAR Collaboration), Phys. G34:S929-930, 2007; J. Bielcikova for the STAR Collaboration, Talk presented at 23rd Winter Workshop on Nuclear Dynamics, Big Sky, Montana, USA, February 11-18, 2007, [arXiv:0707.3100]; J. Bielcikova for the STAR Collaboration, Talk presented at XLIII Rencontres de Moriond, QCD and High Energy Interactions, La Thuile, March 8-15, 2008, [arXiv:0806.2261].
 - [7] B. Abelev (STAR Collaboration), Talk presented at 23rd Winter Workshop on Nuclear Dynamics, Big Sky, Montana, USA, February 11-18, 2007, [arXiv:0705.3371].
 - [8] L. Molnar (STAR Collaboration), J. Phys. G **34**, S593 (2007).
 - [9] R. S. Longacre (STAR Collaboration), Int. J. Mod. Phys. **E16**, 2149 (2007).
 - [10] C. Nattrass (STAR Collaboration), J. Phys. G **35**, 104110 (2008).
 - [11] A. Feng, (STAR Collaboration), J. Phys. G **35**, 104082 (2008).
 - [12] P. K. Netrakanti (STAR Collaboration) J. Phys. G **35**, 104010 (2008).
 - [13] O. Barannikova (STAR Collaboration), J. Phys. G **35**, 104086 (2008).
 - [14] M. Daugherty, (STAR Collaboration), J. Phys. G **35**, 104090 (2008).
 - [15] D. Ray, in Talk presented at Tamura Symposium on Heavy Ion Physics, the University of Texas at Austin, November 2022, 2008,

- <http://www.ph.utexas.edu/~molly/tamura/>.
- [16] D. Kettler, (STAR Collaboration), *Euro. Phys. Jour. C*, **62**, 175 (2009).
 - [17] G. Agakishiev *et al.*, (STAR Collaboration), arXiv:1109.4380 (2011).
 - [18] T. A. Trainor *Phys. Rev. C* **78**, 064908 (2008); T. A. Trainor and D. T. Kettler, *Phys. Rev. D* **74**, 034012 (2006); T. A. Trainor, *Phys. Rev. C* **80**, 044901 (2009); T. A. Trainor, *J. Phys. G* **37**, 085004 (2010).
 - [19] M. van Leeuwen, (STAR Collaboration), *Eur. Phys. J. C* **61**, 569 (2009).
 - [20] A. Adare, *et al.* (PHENIX Collaboration), *Phys. Rev. C* **78**, 014901 (2008).
 - [21] M. P. McCumber (PHENIX Collaboration), *J. Phys. G* **35**, 104081 (2008).
 - [22] Chin-Hao Chen (PHENIX Collaboration), "Studying the Medium Response by Two Particle Correlations", Hard Probes 2008 Intern. Conf. on Hard Probes of High Energy Nuclear Collisions, A Toxa, Galicia, Spain, June 8-14, 2008.
 - [23] Jiangyong Jia, (PHENIX Collaboration), *J. Phys. G* **35**, 104033 (2008).
 - [24] M.J. Tannenbaum, *Eur. Phys. J. C* **61**, 747 (2009).
 - [25] E. Wenger (PHOBOS Collaboration), *J. Phys. G* **35**, 104080 (2008).
 - [26] CMS Collaboration, *JHEP* **1009**, 091 (2010), [arXiv:1009.4122].
 - [27] CMS Collaboration, arXiv:1105.2438 (2011).
 - [28] C. Y. Wong, *Phys. Rev. C* **76**, 054908 (2007).
 - [29] C. Y. Wong, *Chin. Phys. Lett.* **25**, 3936 (2008).
 - [30] C. Y. Wong, *J. Phys. G* **35**, 104085 (2008).
 - [31] C. Y. Wong, *Phys. Rev. C* **78**, 064905 (2008).
 - [32] C. Y. Wong, *Phys. Rev. C* **80**, 034908 (2009).
 - [33] C. Y. Wong, *Phys. Rev. C* **80**, 054917 (2009).
 - [34] C. Y. Wong, *Nonlin. Phenom. Complex Syst.* **12**, 315 (2009), [arXiv:0911.3583].
 - [35] C. Y. Wong, *Phys. Rev. C* **84**, 024901 (2011).
 - [36] E. Shuryak, *Phys. Rec. C* **76**, 047901 (2007).
 - [37] S. A. Voloshin, *Nucl. Phys. A* **749**, 287 (2005).
 - [38] C. B. Chiu and R. C. Hwa *Phys. Rev. C* **79**, 034901 (2009).
 - [39] R. C. Hwa and C. B. Yang, *Phys. Rev. C* **67**, 034902 (2003); R. C. Hwa and Z. G. Tan, *Phys. Rev. C* **72**, 057902 (2005); R. C. Hwa and C. B. Yang, [nucl-th/0602024].
 - [40] C. B. Chiu and R. C. Hwa *Phys. Rev. C* **72**, 034903 (2005).
 - [41] R. C. Hwa, *Phys. Lett.* **B666**, 228 (2008).
 - [42] V. S. Pantuev, [arXiv:0710.1882].
 - [43] A. Dumitru, F. Gelis, L. McLerran, and R. Venugopalan, *Nucl. Phys.* **A810**, 91 (2008).
 - [44] S. Gavin, and G. Moschelli, *J. Phys. G* **35**, 104084 (2008).
 - [45] S. Gavin, L. McLerran, and G. Moschelli, *Phys. Rev. C* **79**, 051902 (2009).
 - [46] N. Armesto, C. A. Salgado, and U. A. Wiedemann, *Phys. Rev. Lett.* **93**, 242301 (2004).
 - [47] P. Romatschke, *Phys. Rev. C* **75**, 014901 (2007).
 - [48] A. Majumder, B. Muller, and S. A. Bass, *Phys. Rev. Lett.* **99**, 042301 (2007).
 - [49] A. Dumitru, Y. Nara, B. Schenke, and M. Strickland, *Phys. Rev. C* **78**, 024909 (2008); B. Schenke, A. Dumitru, Y. Nara, and M. Strickland, *J. Phys. G* **35**, 104109 (2008).
 - [50] R. Mizukawa, T. Hirano, M. Isse, Y. Nara, and A. Ohnishi, *J. Phys. G* **35**, 104083 (2008).
 - [51] Jianyong Jia and R. Lacey, *Phys. Rev. C* **79**, 011901 (2009).
 - [52] Jianyong Jia, *Eur. Phys. J. C* **61**, 255 (2009).
 - [53] Y. Hama, R. P. G. Andrade, F. Grassi, W.-L. Qian, Talk presented at ISMD2010, 21-25 September, 2010, University of Antwerp (Belgium), [arXiv:1012.1342]; R.P.G.Andrade, F.Gardim, F.Grassi, Y.Hama, W.L.Qian [arXiv:1107.0216].
 - [54] A. Dumitru, K. Dusling, F. Gelis, J. Jalilian-Marian, T. Lappi, and R. Venugopalan, *Phys. Lett.* **B697**, 21 (2011), [arXiv:1009.5295].
 - [55] K. Werner, Iu. Karpenko, K. Mikhailov, and T. Pierog [arXiv:1104.3269]; Fu-Ming Liu, K. Werner, [arXiv:1106.5909].
 - [56] R. C. Hwa, C. B. Yang, *Phys. Rev. C* **83**, 024911 (2011), [arXiv:1011.0965].
 - [57] C. B. Chiu and R. C. Hwa, [arXiv:1012.3486].
 - [58] T. A. Trainor, arXiv:1008.4757; T. A. Trainor, arXiv:1011.6351; T. A. Trainor, arXiv:1012.2373.
 - [59] T. A. Trainor and D. T. Kettler, *Phys. Rev. C* **83**, 034903 (2011).
 - [60] T. A. Trainor and D. T. Kettler, arXiv:1010.3048.
 - [61] T. A. Trainor and R. L. Ray, arXiv:1105.5428; R. L. Ray, arXiv:1106.5023.
 - [62] B. Schenke, [arXiv:1106.6012]; B. Schenke, S. Jeon, C. Gale, [arXiv:1109.6289].
 - [63] H. Petersen, C. Greiner, V. Bhattacharya, S. A. Bass, [arXiv:1105.0340].
 - [64] B. A. Arbuzov, E. E. Boos, and V. I. Savrin, [arXiv:1104.1283].
 - [65] M. Yu. Azarkin, I. M. Dremin, and A. V. Leonidov, [arXiv:1102.3258].
 - [66] H. R. Grigoryan, and Y. V. Kovchegov, [arXiv:1012.5431].
 - [67] I. Bautista, J. Dias de Deus, and C. Pajares, [arXiv:1011.1870].
 - [68] I. O. Cherednikov and N. G. Stefanis, [arXiv:1010.4463].
 - [69] I. M. Dremin, and V. T. Kim, [arXiv:1010.0918].
 - [70] E. Levin, A. H. Rezaeian, [arXiv:1105.3275].
 - [71] H. Cheng and T. T. Wu, *Phys. Rev.* **186**, 1611 (1969).
 - [72] H. Cheng and T. T. Wu, *Expanding Protons: Scattering at High Energies*, M. I. T. Press, 1987.
 - [73] Y. J. Feng, O. Hamidi-Ravari, and C. S. Lam, *Phys. Rev. D* **54**, 3114 (1996).
 - [74] Y. J. Feng, O. Hamidi-Ravari, and C. S. Lam, *Phys. Rev. D* **55**, 4016 (1997).
 - [75] C. S. Lam, Lectures given at the First Asia Pacific Workshop on Strong Interactions, Taipei. August 1st to 27th, 1996, hep-ph/9704240.
 - [76] C. S. Lam and K.F. Liu, *Nucl. Phys.* **B 483**, 514 (1997).
 - [77] C. S. Lam and K.F. Liu, *Phys. Rev. Lett.* **79**, 597 (1997).
 - [78] C. S. Lam, *Chin. Jour. Phys.* **35**, 758 (1997), hep-ph/9805210.
 - [79] C. Y. Lo and H. Cheng, *Phys. Rev. D* **13**, 1131 (1976); P. S. Yeung, *Phys. Rev. D* **13**, 23062317 (1976).
 - [80] H. Cheng, J. A. Dickinson, and K. Olaussen, *Phys. Rev. D* **23**, 534 (1981).
 - [81] X. N. Wang and M. Gyulassy, *Phys. Rev. D* **44**, 3501 (1991); X. N. Wang and M. Gyulassy, *Phys. Rev. Lett.* **68**, 1480 (1992).
 - [82] C. Y. Wong, *Phys. Lett. B* **88**, 39 (1979).
 - [83] J. Y. Ollitrault, *Phys. Rev. D* **46**, 229 (1992).
 - [84] S. Voloshin, Y. Zhang, *Phys. Rev. C* **70**, 665 (1996).